INTERNATIONAL JOURNAL OF
NUMERICAL ANALYSIS AND MODELING
Volume 10, Number 1, Pages 203–220

A 2-DIMENSIONAL MECHANICAL MODEL OF THE FORMATION OF A SOMITE

YUKIE GOTO

Abstract. The mechanochemical model proposed in 1983 by G. Oster, J. D. Murray and A. K. Harris has been deployed to describe various morphological phenomena in biology, such as feather bud formation [17] and angiogenesis and vasculogenesis [10, 13]. In this article, we apply a mechanochemical model to the formation of a somite to better understand the role that the mechanical aspects of the cells and the extracellular matrix (ECM) play in somitogensis. In particular, our focus lies in the effect of the contractile forces generated by the cells, which are exerted onto the surrounding ECM. Our approach involves the linear stability analysis and a study of asymptotic behavior of the cell density based on a priori estimates. The full model considered in 2 dimensional space is numerically simulated to show that the traction force of the cells alone can generate a pattern.

Key words. somites, somitogenesis, mechano-chemical model, traction, linear stability analysis, numerical analysis

1. Introduction

Somites are spherical blocks of the mesodermal cells in vertebrate embryos aligning alongside the notochord, which longitudinally extends underneath the neural tube. In later development, they are the precursors to various organs such as ribs, limbs and dorsal skins [25]. Somitogenesis is the formation of these somites and involves a wide range of mechanisms which are spatially and temporally intertwined [1].

At an early developmental stage, the cells in the bilateral bands of the presomitic mesoderm (PSM) express a variety of adhesive molecules on their surfaces depending on their positions. Particularly, those located at the far anterior end of the mesoderm show higher adhesion than those at the posterior end [25]. Consequently, the cells at the anterior end undergo drastic increase in the density and become compacted to much rounder shape, and eventually they separate themselves into a somite at regular time intervals. Throughout the process of somitogenessis, new cells are added in the posterior end of the PSM due to the cell division and the cells entering from Hensen's node, keeping each band of the PSM approximately constant.

The formation of somites are highly regulated in terms of space and time. Each somite is periodically formed in pair on both sides of the notochord from the anterior end to the posterior end of the PSM [24, 25]. For example, the amount of time required for one somite to form is approximately 30 minutes in case of zebrafish and, for the chick embryo 90 minutes and for the mouse embryo 120 minutes. Furthermore, the total number of somites is characteristic to species: 30, 50 and 65 somites for Zebrafish, chick and mouse embryo, respectively, [8, 24]

There have been several models proposed to explain the formation of somites, among which are the clock and wavefront model first proposed by Cookee and Zeeman [3] and later revised by Pourquié et al. [5, 6], the wave/cell polarization

Received by the editors December 1, 2011 and, in revised form, December 22, 2011.
2000 *Mathematics Subject Classification.* 92C15, 35Q80.

model proposed by Polezhaev [19, 20], the Reaction-diffusion model proposed by Meinhardt [12], and the cell-cycle model proposed by Stern et al.[21, 22] and later mathematically formulated by Colliers and his co-workers [2, 11]. The model which we choose to study in this paper is the mechanochemical model, applied to somitogenesis. This model was first introduced by J. D. Murray, G. F. Oster and A. K. Harris in 1983, see [17], and there have been various applications of this model to morphogenetic pattern formation [10, 14, 15, 17, 18, 23]. Compared to the other models mentioned earlier, this model focuses on the mechanical aspects of the cells and their surrounding environment and relies on the measurable quantities such as tissue deformation properties, cell densities and forces [15, 16, 17].

This article is organized as follows. In Section 2, we give a brief overview of the mechanical properties of the mesodermal cells and the ECM and that of their mechanical interaction, followed by the introduction of a mechanochemical model in the context of somitogenesis along with the short explanation of its construction. Then, in Section 3, the linear stability analysis is performed and asymptotic behavior of the cell density is analyzed via linearization of the system and a priori estimates. Finally, in Section 4, we show the discretization of the system and the results of our numerical simulation.

2. Mechanochemical model

The fibroblast cells live and crawl within the fibrous tissue composed of the extracellular matrix (ECM). Their interaction with the surrounding environment can lead to a morphogenic pattern formation in an embryo at an early developmental stage. The characteristic features which enable the cells to move within the fibrous surroundings are broad and flat protrusions, called lamellipodia, and long finger-like protrusions, called filopodia, which extend from the lamellipodia. The filopodia are often assumed to sense the surface of the environment to look for guidance cues. However, since the precise functionalities of the two remain elusive, we will not make distinction between the roles each one takes upon locomotion of the cells. The filopodia (lamellipodia) can attach themselves to the surrounding adhesive sites which include the ECM material points and the surfaces of other cells and then, contract. Since the filopodia extend to all the opposing directions, the resulting situation is just like a tug-of-war and so, the cell migrates in the direction of the net contractile (traction) force. In accordance to the translocation of the cells, the ECM provides further geometric guidance cues directing the cells' movement.

This intricately coordinated mechanical interaction between the cells and the viscoelastic ECM is encapsulated in the mechano-chemical model [17]. In this paper, we will make use of this framework to find out whether the mechanical interaction of the cells with their surrounding environment alone can lead to the formation of a somite. To be more precise, we will numerically experiment to see if the traction forces exerted by the cells onto the ECM are enough to generate a somite.

Now let us introduce the mechanochemical model. Let $\Omega = (0, L_1) \times (0, L_2)$ where L_1, $L_2 > 0$. For each $\mathbf{x} = (x, y) \in \Omega$ and $t > 0$, we define the three variables

$$
\begin{aligned}
&n = n(\mathbf{x}, t) = \text{ the density of cells (cells/cm}^3\text{)},\\
&\rho = \rho(\mathbf{x}, t) = \text{ the density of ECM (mg /cm}^3\text{)},\\
&\mathbf{u} = \mathbf{u}(\mathbf{x}, t) = \text{ the displacement vector of the ECM.}
\end{aligned}
\tag{1}
$$

With these unknowns, the model reads

$$\begin{cases} n_t = -\nabla \cdot (n\mathbf{u}_t)\,, \\ \nabla \cdot \left[(\mu_1 \epsilon_t + \mu_2 \theta_t I) + \dfrac{E}{1+\nu}\left(\epsilon + \dfrac{\nu}{1-2\nu}\theta I\right) + \dfrac{\tau n \rho}{1+\lambda n^2} I \right] = 0, \\ \rho_t = -\nabla \cdot (\rho \mathbf{u}_t)\,, \end{cases} \tag{2}$$

where ϵ is the strain tensor defined by $\epsilon = \epsilon(\mathbf{u}) = \frac{1}{2}\left(\nabla \mathbf{u} + \nabla \mathbf{u}^T\right)$, $\theta = \nabla \cdot \mathbf{u}$ is the dilation of the matrix material, $\lambda > 0$ and

$$\tau := \tau(x,y) = \frac{\tau_{som}}{1 + e^{-2\alpha(x-x^*)}} + \tau_{psm}, \qquad \tau_{psm},\, \tau_{som},\, \alpha,\, x^* > 0. \tag{3}$$

Furthermore, each parameter represents the following quantities:

$$\begin{aligned} \mu_1 &= \text{ the shear viscosity,} \\ \mu_2 &= \text{ the bulk viscosity,} \\ E &= \text{ Young's modulus,} \\ \nu &= \text{ Poisson ratio,} \\ I &= \text{ the unit tensor.} \end{aligned} \tag{4}$$

The relations between the coefficients μ_1, μ_2, E and ν are well-known and available in the literature.

Below we provide a brief description of each of the three equations. For the detailed construction of the equations, we refer the readers to [15, 17]; $(2)_1$ is the cell equation, describing the movement of the cells within the ECM. Assuming that the proliferation and both short-range and long-range diffusions of the cells are negligible, this equation reflects in a classical manner the transportation of the cells by the displacement of the ECM. Similarly, $(2)_3$ is the conservation equation for the ECM, representing its convection movement; $(2)_2$ is a tensorial equation depicting the mechanical equilibrium between the ECM and the traction forces exerted by the cells. Assuming that the ECM material can be modeled as a linear isotropic viscoelastic continuum and that the cells and the ECM remain in the mechanical equilibrium, this equation is derived from applying the fundamental law on continuum mechanics:

$$\nabla \cdot \sigma + \rho F = 0. \tag{5}$$

where σ is the stress tensor and F is the external force exerted on the matrix. In our case, σ can be expressed as the sum of the two stress tensors depending on its respective contributor: σ_{ECM} and σ_{cell}. Since the ECM is assumed to possess the viscous and elastic properties, σ_{ECM} is defined by

$$\sigma_{\text{ECM}} = \mu_1 \epsilon_t + \mu_2 \theta_t I + \frac{E}{1+\nu}\left(\epsilon + \frac{\nu}{1-2\nu}\theta I\right). \tag{6}$$

To consider σ_{cell}, we identify the adhesive sites for the filopodia with the surfaces of neighboring cells and the ECM material points and thus, consequently, on a region where n and ρ are large, the filopodia gain more traction. We also note that there is experimental data indicating that there is adhesion gradient increasing from the posterior end to the anterior end of the presomitic mesoderm (PSM), we obtain σ_{cell} defined by

$$\sigma_{\text{cell}} = \frac{\tau n \rho}{1+\lambda n^2} I, \tag{7}$$

where τ is defined as in (3). Finally, assuming the external forces F is negligible, the substitution of (6) and (7) into (5) leads to $(2)_2$.

In order to proceed with the mathematical analysis, we equip the system (2) with the initial conditions given by

$$n(x,y,0)=n_0,\quad \rho(x,y,0)=\rho_0,\quad \mathbf{u}(x,y,0)=(0,0), \tag{8}$$

where n_0, $\rho_0>0$ are constant, and with the following boundary conditions: zero-flux boundary conditions for n and ρ,

$$\frac{\partial n}{\partial \mathbf{n}}=0,\quad \frac{\partial \rho}{\partial \mathbf{n}}=0 \text{ for } (x,y)\in\partial\Omega, \tag{9}$$

and the zero boundary condition for $\mathbf{u}$,

$$\mathbf{u}(x,y)=(0,0) \text{ for } (x,y)\in\partial\Omega. \tag{10}$$

We integrate $(2)_1$ and $(2)_3$ over Ω. With the use of integration by parts and the imposed boundary conditions, we find

$$\frac{d}{dt}\int_\Omega n(\mathbf{x},t)d\mathbf{x}=0 \quad \text{and} \quad \frac{d}{dt}\int_\Omega \rho(\mathbf{x},t)d\mathbf{x}=0, \tag{11}$$

where $\mathbf{x}=(x,y)$. For the cell-ECM interaction equation $(2)_2$, we multiply it by $\mathbf{u}$ and then integrate over Ω. It then follows from the integration by parts and the boundary conditions that

$$\begin{aligned}
&\frac{\mu_1}{4}\frac{d}{dt}\int_\Omega |\nabla\mathbf{u}|^2d\mathbf{x}+\Big(\frac{\mu_1}{4}+\frac{\mu_2}{2}\Big)\frac{d}{dt}\int_\Omega |\nabla\cdot\mathbf{u}|^2d\mathbf{x}\\
&\quad+\frac{E}{2(1+\nu)}\int_\Omega |\nabla\mathbf{u}|^2d\mathbf{x}+\frac{E}{2(1+\nu)(1-2\nu)}\int_\Omega |\nabla\cdot\mathbf{u}|^2d\mathbf{x}\\
&\qquad+\int_0^{L_2}(\tau(0)-\tau(L_1))\frac{n(0,y,t)\rho(0,y,t)}{1+\lambda(n(0,y,t))^2}u(0,y,t)dy\\
&\qquad+\int_\Omega\frac{\tau n\rho}{1+\lambda n^2}\nabla\cdot\mathbf{u}d\mathbf{x}=0,
\end{aligned} \tag{12}$$

where we have set $\mathbf{u}=(u,v)$ and defined $|\nabla\mathbf{u}|^2:=|\nabla u|^2+|\nabla v|^2$.

These a priori estimates are not sufficient to derive an existence and uniqueness result of solutions in the present nonlinear problem. However, in modeling the formation of a pattern, the system (2) must admit spatially and temporally inhomogeneous solutions which correspond to the cell aggregation. In order to see if there is still some potential, in the next section we perform the stability analysis by spectral method around a uniform steady state solution and then test the validity of its prediction by numerical simulation.

3. Mathematical analysis on the mechanochemical model

3.1. Linear stability analysis. Let us first bring our attention to the function τ defined in (3), which involves our control parameters. The parameter x^* splits the domain Ω into two regions: $\{(x,y): x^*\le x\le L_1,\ 0\le y\le L_2\}$ corresponds to the somitic region where a somite is formed and $\{(x,y): 0\le x<x^*,\ 0\le y\le L_2\}$ corresponds to the (non-somitic) PSM. Also, α controls the sharpness of the increase of τ from the PSM region to the somitic region. Most importantly, the parameters of our main interest are τ_{som} and τ_{psm}. The values of these two parameters determine the magnitude of the cell traction forces exerted on the surrounding adhesive sites. The question to be answered is how large or small they have to be in the somitic region or in the PSM, respectively. The following linear stability analysis suggests a threshold value $\tau_{critical}>0$ for the traction force.

For further analysis, in order to avoid cumbersome notations, we rewrite the system (2) by using the Einstein notation as follows;

$$
\begin{cases}
n_t = -(n\partial_t u_j)_{,j}\,, \\
\dfrac{\partial}{\partial t}\left[\dfrac{\mu_1}{2}u_{k,jj} + \left(\dfrac{\mu_1}{2}+\mu_2\right)u_{j,jk}\right] \\
\qquad\qquad + \dfrac{E}{2(1+\nu)}u_{k,jj} + \dfrac{E}{2(1+\nu)(1-2\nu)}u_{j,jk} + \left(\dfrac{\tau n\rho}{1+\lambda n^2}\right)_{,k} = 0 \\
\qquad\qquad\qquad\qquad\qquad\qquad\qquad\qquad \text{for } k = 1,2,3, \\
\rho_t = -(\rho\partial_t u_j)_{,j}\,.
\end{cases} \tag{13}
$$

The stability analysis by spectral method naturally imposes the space-periodic boundary conditions. That is,

$$
\begin{aligned}
&n(0,y,t) = n(L_1,y,t) \text{ and } n(x,0,t) = n(x,L_2,t), \\
&\mathbf{u}(0,y,t) = \mathbf{u}(L_1,y,t) \text{ and } \mathbf{u}(x,0,t) = \mathbf{u}(x,L_2,t), \\
&\rho(0,y,t) = \rho(L_1,y,t) \text{ and } \rho(x,0,t) = \rho(x,L_2,t).
\end{aligned} \tag{14}
$$

Moreover, we assume that τ is a constant

The uniform steady state solutions to the above set of equations are of the form

$$
n = n_0, \qquad \rho = \rho_0, \qquad \mathbf{u} = \mathbf{u}_0\,, \tag{15}
$$

where n_0, ρ_0 and $\mathbf{u}_0 = (u_0, v_0)$ are constants. Among all the possible values of n_0, ρ_0 and $\mathbf{u}_0$, $n_0 \leq 0$ and $\rho_0 \leq 0$ are irrelevant in the biological situation we are considering here and so, we will take n_0, $\rho_0 > 0$. Also, we set $\mathbf{u}_0 = (0,0)$. The fundamental idea behind the linear stability analysis is to analytically observe the behavior of the solutions when a small perturbation is imposed on their steady states. Thus, we let

$$
n = n_0 + \tilde{n}, \qquad \rho = \rho_0 + \tilde{\rho}, \qquad \mathbf{u} = \tilde{\mathbf{u}}\,, \tag{16}
$$

where $\tilde{n}$, $\tilde{\rho}$ and $\tilde{\mathbf{u}}$ satisfy $|\tilde{n}| \ll n_0$, $|\tilde{\rho}| \ll \rho_0$ and $|\tilde{\mathbf{u}}| \ll n_0^{-\frac{1}{3}}$, respectively. We then substitute these into (13) and after ignoring the nonlinear terms, we find the linearized system as follows;

$$
\begin{cases}
\partial_t\tilde{n} = -n_0\partial_t\tilde{u}_{j,j}\,, \\
\dfrac{\partial}{\partial t}\left[\dfrac{\mu_1}{2}\tilde{u}_{k,jj} + \left(\dfrac{\mu_1}{2}+\mu_2\right)\tilde{u}_{j,jk}\right] + \dfrac{E}{2(1+\nu)}\tilde{u}_{k,jj} + \dfrac{E}{2(1+\nu)(1-2\nu)}\tilde{u}_{j,jk} \\
\qquad\qquad + \dfrac{\tau\rho_0(1-\lambda n_0^2)}{(1-\lambda n_0^2)^2}\tilde{n}_{,k} + \dfrac{\tau n_0}{1-\lambda n_0^2}\tilde{\rho}_{,k} = 0 \quad \text{for } k = 1,2,3, \\
\partial_t\tilde{\rho} = -\rho_0\partial_t\tilde{u}_{j,j}\,.
\end{cases} \tag{17}
$$

Note that $(17)_2$ is obtained by linearizing only the term corresponding to σ_{cell}, since the derivatives of $\mathbf{u}$ are linearly involved in $(13)_2$.

Now we look for a solution (17) of the form

$$
\tilde{n} = \tilde{N}e^{\sigma t + i\omega\cdot\mathbf{x}}\,, \qquad \tilde{\rho} = \tilde{P}e^{\sigma t + i\omega\cdot\mathbf{x}}\,, \qquad \tilde{\mathbf{u}} = \tilde{\mathbf{U}}e^{\sigma t + i\omega\cdot\mathbf{x}}\,, \tag{18}
$$

where σ is the growth factor, $\omega = (\omega_1, \omega_2, \omega_3)$ is the wavevector and $\tilde{N}$, $\tilde{P}$ and $\tilde{\mathbf{U}} = (\tilde{U}_1, \tilde{U}_2, \tilde{U}_3)$ are proportionality coefficients. Substituting (18) into (17), we

find

(19)
$$\begin{cases} \tilde{N} + in_0\omega_j\tilde{U}_j = 0\,, \\ \left[\left\{\left(\dfrac{\mu_1}{2}+\mu_2\right)\omega_k^2 + \dfrac{\mu_1}{2}\omega_j\omega_j\right\}\sigma + \dfrac{E}{2(1+\nu)(1-2\nu)}\omega_k^2 + \dfrac{E}{2(1+\nu)}\omega_j\omega_j\right]\tilde{U}_k \\ \qquad + \left[\left(\dfrac{\mu_1}{2}+\mu_2\right)\sigma + \dfrac{E}{2(1+\nu)(1-2\nu)}\right]\displaystyle\sum_{j\neq k}\omega_j\omega_k\tilde{U}_j \\ \qquad\qquad - i\dfrac{\tau\rho_0(1-\lambda n_0^2)}{(1+\lambda n_0^2)^2}\omega_k\tilde{N} - i\dfrac{\tau n_0}{1+\lambda n_0^2}\omega_k\tilde{P} = 0 \quad \text{for } k=1,2,3, \\ \tilde{P} + i\rho_0\omega_j\tilde{U}_j = 0\,. \end{cases}$$

This is a system of five linear equations with unknowns $\tilde{N}$, $\tilde{P}$, $\tilde{U}_1$, $\tilde{U}_2$ and $\tilde{U}_3$. For this system to have a nontrivial solution, we require that the determinant of the corresponding 5 by 5 matrix to be zero. Equivalently,

$$b_3\sigma^3 + b_2\sigma^2 + b_1\sigma + b_0 = 0\,, \tag{20}$$

with

$$\begin{aligned} b_3 &= -\frac{1}{4}\mu_1^2(\mu_1+\mu_2)|\omega|^6, \\ b_2 &= \mu_1\left[\frac{\mu_1 E(5\nu-3)+\mu_1\tilde{\tau}(1+\nu)(1-2\nu)+2\mu_2 E(2\nu-1)}{4(1+\nu)(1-2\nu)}\right]|\omega|^6, \\ b_1 &= E\left[\frac{\mu_1 E(4\nu-3)+2\mu_1\tilde{\tau}(1+\nu)(1-2\nu)+\mu_2 E(2\nu-1)}{4(1+\nu)^2(1-2\nu)}\right]|\omega|^6, \\ b_0 &= E^2\left[\frac{E(\nu-1)+\tilde{\tau}(1+\nu)(1-2\nu)}{4(1+\nu)^3(1-2\nu)}\right]|\omega|^6, \end{aligned} \tag{21}$$

and with

$$|\omega| = \omega_1+\omega_2+\omega_3 \text{ and } \tilde{\tau} = \frac{2\tau n_0 p_0}{(1+\lambda n_0^2)^2}; \tag{22}$$

(20) together with (21) is called the dispersion relation and its roots are given by

$$\sigma_1,\,\sigma_2 = -\frac{E}{\mu_1(1+\nu)} \text{ and } \sigma_3 = \frac{1}{\mu_1+\mu_2}\left(\frac{E(\nu-1)}{(1+\nu)(1-2\nu)}+\tilde{\tau}\right). \tag{23}$$

The formation of a somite requires that (19) admits spatially inhomogeneous solutions which do not decay with time. Thus, we need to obtain the solution σ of (20) such that $\mathrm{Re}(\sigma) > 0$, since this condition leads to instability modes. Now, we observe that σ_1, $\sigma_2 < 0$ since μ_1, E, $\nu > 0$ and hence, they are not of our interest. On the other hand, $\sigma_3 > 0$ if and only if

$$\tau > \tau_{critical} \tag{24}$$

where $\tau_{critial}$ is defined by

$$\tau_{critical} := \frac{E(1-\nu)}{(1+\nu)(1-2\nu)}\frac{(1+\lambda n_0^2)^2}{2n_0\rho_0}\,. \tag{25}$$

Note that $\tau_{critical} > 0$ since typically $0 < \nu < 0.5$.

We can then deduce the following. A necessary condition for the formation of a somite is that the traction force exerted by the fibroblast cells onto the ECM must

exceed the value of $\tau_{critical}$. That is, if the values of τ_{som} and τ_{psm} are chosen so that

$$\begin{aligned} &\tau(x,y) \le \tau_{critial} \text{ for } 0 \le x < x^* \text{ and } 0 \le y \le L_2 \\ &\tau(x,y) \ge \tau_{critial} \text{ for } x^* \le x \le L_1 \text{ and } 0 \le y \le L_2, \end{aligned} \tag{26}$$

then we can expect the aggregation of cells in the somitic region.

3.2. Asymptotic development of the cell density. In this section, we study the time evolution of the model (2), in particular, that of the cell density n, using two different approaches: One is based on a priori estimate and the other involves a method of perturbation analysis. These two approaches shed some light on the asymptotic behavior of n and demonstrate how the different parameters play a role in controlling its amplitude.

In order to proceed, we will first reduce the above set (2) of four coupled nonlinear partial differential equations into one as demonstrated below.

Taking the divergence of $(2)_1$, the tensorial equation can be expressed in terms of θ:

$$\frac{\partial}{\partial t}\Delta\theta + \frac{E(1-\nu)}{(1+\nu)(1-2\nu)}\Delta\theta + \Delta\left(\frac{\tau n\rho}{1+\lambda n^2}\right) = 0. \tag{27}$$

Since the changes in cell strain during pattern formation in an embryo is small [4, Sec 5], we assume as in [4] that $|\theta| \ll 1$. We can then linearize $(2)_1$ and $(2)_2$ about the respective uniform steady states, n_0 and ρ_0. Integrating the resulting equations over $[0,t]$, we find that

$$n(\mathbf{x},t) = n_0(1-\theta(\mathbf{x},t)) \text{ and } \rho(\mathbf{x},t) = \rho_0(1-\theta(\mathbf{x},t)). \tag{28}$$

Solving $(28)_1$ for θ and then substituting the resulting equation into $(28)_2$ leads to an expression of ρ in terms of n. Thus, combining (27) with (28), we obtain the small-strain quasi-steady state equation which involves only n:

$$(\mu_1+\mu_2)\frac{\partial}{\partial t}\Delta n + \frac{E(1-\nu)}{(1+\nu)(1-2\nu)}\Delta n - \Delta\left(\frac{\tau\rho_0 n^2}{1+\lambda n^2}\right) = 0. \tag{29}$$

Here we recall that τ is assumed to be a positive constant as in Sec 3.1, λ is one of the control parameters and ρ_0, μ_1, μ_2, E and ν are constants.

In order to investigate the asymptotic behavior of n, we work on the above equation (29). Our first approach involves establishing a priori estimate and to begin, we multiply (29) by n and integrate over Ω. Using the integration by parts together with the boundary condition (9), we find

$$\begin{aligned} \frac{\mu_1+\mu_2}{2}\frac{d}{dt}\int_\Omega |\nabla n(\mathbf{x},t)|^2 d\mathbf{x} + \frac{E(1-\nu)}{(1+\nu)(1-2\nu)}\int_\Omega |\nabla n(\mathbf{x},t)|^2 d\mathbf{x} \\ - 2\tau\rho_0\int_\Omega \frac{n}{(1+\lambda n^2)^2}|\nabla n(\mathbf{x},t)|^2 d\mathbf{x} = 0. \end{aligned} \tag{30}$$

Since for all $n \in \mathbb{R}$,

$$-c_1(\lambda) \le \frac{n}{(1+\lambda n^2)^2} \le c_1(\lambda) \text{ where } c_1(\lambda) := \frac{9}{16\sqrt{3\lambda}}, \tag{31}$$

it follows that

$$\begin{aligned} &\frac{\mu_1+\mu_2}{2}\frac{d}{dt}\int_\Omega |\nabla n(\mathbf{x},t)|^2 d\mathbf{x} \\ &\qquad \le \left(2\tau\rho_0 c_1(\lambda) - \frac{E(1-\nu)}{(1+\nu)(1-2\nu)}\right)\int_\Omega |\nabla n(\mathbf{x},t)|^2 d\mathbf{x}. \end{aligned} \tag{32}$$

Application of Gronwall's inequality results in

(33)
$$\frac{d}{dt}\int_\Omega |\nabla n(\mathbf{x},t)|^2 d\mathbf{x} \leq \int_\Omega |\nabla n(\mathbf{x},0)|^2 d\mathbf{x}\left\{\exp\left[\frac{2}{\mu_1+\mu_2}\left(2\tau\rho_0 c_1(\lambda) - \frac{E(1-\nu)}{(1+\nu)(1-2\nu)}\right)t\right]\right\}.$$

We note that by (25) and (31),

$$\frac{2}{\mu_1+\mu_2}\left(2\tau\rho_0 c_1(\lambda) - \frac{E(1-\nu)}{(1+\nu)(1-2\nu)}\right) > 0 \text{ if and only if } \tau > \tau_{critial}\,. \tag{34}$$

It follows from (33) that if the initial data $n(\mathbf{x},0)$ is constant as in (8), then n is a function constant in $\mathbf{x}$. On the other hand, if the initial data $n(\mathbf{x},0)$ is not a constant function of $\mathbf{x}$, then $|\nabla n(t)|_{L^2(\Omega)}$ tends to 0 exponentially as t increases, provided $\tau < \tau_{critical}$. If $\tau > \tau_{critial}$, then there is possibility that $|\nabla n(t)|_{L^2(\Omega)}$ grows exponentially as t increases.

The next approach focus on the long time behavior of n when the traction function is perturbed from $\tau_{critical}$. Thus, given $0 < \epsilon \ll 1$, we set

$$T = \epsilon^2 t \text{ and } \tau = \tau_{critical} + \epsilon^2\delta, \text{ where } \delta = \pm 1, \tag{35}$$

and view n as a function of ϵ, $\mathbf{x}$ and T, ignoring the dependence of n on t except through T. We then substitute (35) into the linearized equation of (29). Using (25) and $\frac{\partial}{\partial t} = \epsilon^2\frac{\partial}{\partial T}$, we find

$$(\mu_1+\mu_2)\frac{\partial}{\partial T}\Delta n - \delta\frac{2\rho_0 n_0}{(1+\lambda n_0^2)^2}\Delta n = 0. \tag{36}$$

Thus, we see that for $T > 0$, the cell density n satisfies the following elliptic equation;

$$\Delta n(\mathbf{x},T) = \Delta n(\mathbf{x},0)\exp\left[\delta\frac{2n_0\rho_0}{(\mu_1+\mu_2)(1+\lambda n_0^2)^2}T\right], \qquad \mathbf{x}\in\Omega. \tag{37}$$

It can be inferred from the above equation that, if the given initial data $n(\mathbf{x},0)$ is a constant function over Ω, then $n(\mathbf{x},T) = C(T)$ for some function C. If otherwise, as T increases, Δn grows exponentially when $\tau > \tau_{critical}$ (*i.e.*, $\delta = 1$) and it decreases exponentially when $\tau < \tau_{critical}$ (*i.e.*, $\delta = -1$).

4. Numerical simulation

In order to test what is predicted by linear stability analysis, we consider the problem (2) over the domain $\Omega = [0,10]\times[0,1]$, *i.e.,* $L_1 = 10$ and $L_2 = 1$. Also, as stated in Section 2, we impose zero-flux boundary conditions (9) for n and ρ and the zero boundary condition (10) for $\mathbf{u}$. The initial conditions are chosen to correspond to the uniform steady states, $n(x,y,0) = n_0$, $\rho(x,y,0) = \rho_0$ and $\mathbf{u}(x,y,0) = (0,0)$.

A typical graph of the traction function is given below. Here we have set $\tau_{som} = 6.43\times10^6$, $\tau_{psm} = 3.21\times10^6$, $x^* = 5$ and $\alpha = 1$.

4.1. Discretizations. For discretizing a domain, we introduce M meshlines parallel to y-axis and N meshlines parallel to x-axis, which subdivide the computational domain Ω into $(M+1)\times(N+1)$ many rectangular meshes. The size of each mesh is then Δx by Δy where $\Delta x = \frac{10}{M+1}$ and $\Delta y = \frac{1}{N+1}$ for some integers M, $N > 0$. We set $x_0 = 0$, $x_{M+1} = L_1$, $y_0 = 0$ and $y_{N+1} = L_2$ and define the nodal points

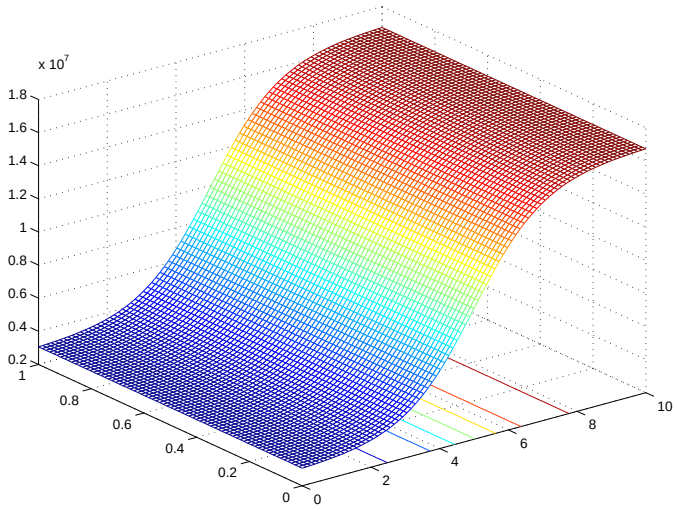

FIGURE 1. Traction function.

by $x_i = i\Delta x$ for $i = 1, 2, \ldots, M$ and $y_j = j\Delta y$ for $j = 1, 2, \ldots, N$. Denoting a time-step by Δt, we can write

$$n^k_{i,j} \approx n(i\Delta x, j\Delta y, k\Delta t), \quad \rho^k_{i,j} \approx n(i\Delta x, j\Delta y, k\Delta t), \tag{38}$$

and if $\mathbf{u} = (u, v)$,

$$\mathbf{u}^k_{i,j} \approx (u^k_{i,j}, v^k_{i,j}) \approx (\, u(i\Delta x, j\Delta y, k\Delta t), v(i\Delta x, j\Delta y, k\Delta t)\,)\,. \tag{39}$$

We discretize the cell equation $(2)_1$ and the ECM equation $(2)_2$ by using implicit Euler method for time derivatives of n and ρ, centered finite difference for space derivatives $\nabla\cdot$ and backward difference for $\mathbf{u}_t$. Then, the discretized cell equation reads: for $k = 0, 1, 2, \ldots$, $i = 1, \ldots, M$ and $j = 1, \ldots N$,

$$\begin{aligned} n^{k+1}_{i,j} &- \frac{1}{2\Delta y}(v^{k+1}_{i,j-1} - v^k_{i,j-1})n^{k+1}_{i,j-1} - \frac{1}{2\Delta x}(u^{k+1}_{i-1,j} - u^k_{i-1,j})n^{k+1}_{i-1,j} \\ &+ \frac{1}{2\Delta y}(v^{k+1}_{i,j+1} - v^k_{i,j+1})n^{k+1}_{i,j+1} + \frac{1}{2\Delta x}(u^{k+1}_{i+1,j} - u^k_{i+1,j})n^{k+1}_{i+1,j} = n^k_{i,j} \end{aligned} \tag{40}$$

This results in a $MN \times MN$ linear matrix system:

$$\mathcal{A}N^{k+1} = N^k, \tag{41}$$

where N^k is a vector of length MN defined by

$$N^k = (n^k_{1,1}, n^k_{2,1}, \ldots, n^k_{M,1}, n^k_{2,1}, n^k_{2,2}, \ldots, n^k_{M,2} \ldots, n^k_{1,N}, n^k_{2,N}, \ldots, n^k_{M,N}) \tag{42}$$

and A is a $MN \times MN$ matrix of the form given by

$$\mathcal{A} = \begin{pmatrix} D_1 & S_1 & 0 & \cdots & 0 \\ T_1 & D_2 & S_2 & \ddots & \vdots \\ 0 & T_2 & D_3 & \ddots & 0 \\ \vdots & \ddots & \ddots & \ddots & S_{N-1} \\ 0 & \cdots & 0 & T_{N-1} & D_N \end{pmatrix} \tag{43}$$

with D_l being an $M \times M$ tridiagonal matrix for $l = 1, \ldots, M$ and S_l, T_l begin $M \times M$ diagonal matrices. For fixed i, j and k, (40) corresponds to $((j-1)M + i)^{\text{th}}$-row of

the matrix $\mathcal{A}$. We discretize the ECM equation $(2)_2$ in the same manner and arrive at

$$\begin{aligned}(44)\qquad &\rho_{i,j}^{k+1}-\frac{1}{2\Delta y}(v_{i,j-1}^{k+1}-v_{i,j-1}^{k})\rho_{i,j-1}^{k+1}-\frac{1}{2\Delta x}(u_{i-1,j}^{k+1}-u_{i-1,j}^{k})\rho_{i-1,j}^{k+1}\\ &+\frac{1}{2\Delta y}(v_{i,j+1}^{k+1}-v_{i,j+1}^{k})\rho_{i,j+1}^{k+1}+\frac{1}{2\Delta x}(u_{i+1,j}^{k+1}-u_{i+1,j}^{k})\rho_{i+1,j}^{k+1}=\rho_{i,j}^{k}.\end{aligned}$$

As in the case of the cell equation, this leads to an $MN\times MN$ linear matrix system given by $\mathcal{A}P^{k+1}=P^{k}$ where $\mathcal{A}$ is defined as in 43 and

$$(45)\qquad P^{k}=(\rho_{1,1}^{k},\rho_{2,1}^{k},\dots,\rho_{M,1}^{k},\rho_{2,1}^{k},\rho_{2,2}^{k},\dots,\rho_{M,2}^{k}\dots,\rho_{1,N}^{k},\rho_{2,N}^{k},\dots,\rho_{M,N}^{k})\,.$$

For the cell-ECM interaction equation $(2)_3$, we first employ the explicit Euler method for time derivative and then centered finite difference for space derivatives. We then obtain two sets of equations; for $i=1,\dots,M$ and $j=1,\dots,N$,

$$\begin{aligned}(46)\qquad &\alpha_{i,j}^{u}u_{i,j}^{k+1}+\alpha_{i,j-1}^{u}u_{i,j-1}^{k+1}+\alpha_{i-1,j}^{u}u_{i-1,j}^{k+1}+\alpha_{i,j+1}^{u}u_{i,j+1}^{k+1}+\alpha_{i+1,j}^{u}u_{i+1,j}^{k+1}\\ &\qquad+c^{R}\left(v_{i-1,j-1}^{k+1}-v_{i-1,j+1}^{k+1}+v_{i+1,j+1}^{k+1}-v_{i+1,j-1}^{k+1}\right)\\ &=\beta_{i,j}^{u}u_{i,j}^{k}+\beta_{i,j-1}^{u}u_{i,j-1}^{k}+\beta_{i-1,j}^{u}u_{i-1,j}^{k}+\beta_{i,j+1}^{u}u_{i,j+1}^{k}+\beta_{i+1,j}^{u}u_{i+1,j}^{k}\\ &\qquad+c^{L}\left(v_{i-1,j-1}^{k}-v_{i-1,j+1}^{k}+v_{i+1,j+1}^{k}-v_{i+1,j-1}^{k}\right)+f_{(j-1)M+i}^{k}\end{aligned}$$

and

$$\begin{aligned}(47)\qquad &\alpha_{i,j}^{v}v_{i,j}^{k+1}+\alpha_{i,j-1}^{v}v_{i,j-1}^{k+1}+\alpha_{i-1,j}^{v}v_{i-1,j}^{k+1}+\alpha_{i,j+1}^{v}v_{i,j+1}^{k+1}+\alpha_{i+1,j}^{v}v_{i+1,j}^{k+1}\\ &\qquad+c^{R}\left(u_{i-1,j-1}^{k+1}-u_{i-1,j+1}^{k+1}+u_{i+1,j+1}^{k+1}-u_{i+1,j-1}^{k+1}\right)\\ &=\beta_{i,j}^{v}v_{i,j}^{k}+\beta_{i,j-1}^{v}v_{i,j-1}^{k}+\beta_{i-1,j}^{v}v_{i-1,j}^{k}+\beta_{i,j+1}^{v}v_{i,j+1}^{k}+\beta_{i+1,j}^{v}v_{i+1,j}^{k}\\ &\qquad+c^{L}\left(u_{i-1,j-1}^{k}-u_{i-1,j+1}^{k}+u_{i+1,j+1}^{k}-u_{i+1,j-1}^{k}\right)+f_{MN+(j-1)M+i}^{k},\end{aligned}$$

where the coefficients in the left hand sides of the above two equations are given by

$$\begin{aligned}(48)\qquad \alpha_{i,j}^{u}&=\frac{-2(\mu_1+\mu_2)(\Delta y)^2-\mu_1(\Delta x)^2}{(\Delta x)^2(\Delta y)^2},\\ \alpha_{i,j-1}^{u}&=\alpha_{i,j+1}^{u}=\frac{\mu_1}{2(\Delta y)^2},\\ \alpha_{i-1,j}^{u}&=\alpha_{i+1,j}^{u}=\frac{\mu_1+\mu_2}{(\Delta x)^2},\\ \alpha_{i,j}^{v}&=\frac{-2(\mu_1+\mu_2)(\Delta x)^2-\mu_1(\Delta y)^2}{(\Delta x)^2(\Delta y)^2},\\ \alpha_{i,j-1}^{v}&=\alpha_{i,j+1}^{v}=\frac{\mu_1+\mu_2}{(\Delta y)^2},\\ \alpha_{i-1,j}^{v}&=\alpha_{i+1,j}^{v}=\frac{\mu_1}{2(\Delta x)^2},\\ c^{R}&=\frac{1}{4\Delta x\Delta y}\left(\frac{\mu_1}{2}+\mu_2\right),\end{aligned}$$

and those in the right hand sides are given by

(49)
$$\beta^u_{i,j} = \frac{2}{(\Delta x)^2}\left[\Delta t\frac{E(1-\nu)}{(1+\nu)(1-2\nu)} - (\mu_1+\mu_2)\right] + \frac{2}{(\Delta y)^2}\left[\Delta t\frac{E}{2(1+\nu)} - \frac{\mu_1}{2}\right],$$
$$\beta^u_{i,j-1} = \beta^u_{i,j+1} = -\frac{1}{(\Delta y)^2}\left[\Delta t\frac{E}{2(1+\nu)} - \frac{\mu_1}{2}\right],$$
$$\beta^u_{i-1,j} = \beta^u_{i+1,j} = -\frac{1}{(\Delta x)^2}\left[\Delta t\frac{E(1-\nu)}{(1+\nu)(1-2\nu)} - (\mu_1+\mu_2)\right],$$
$$\beta^v_{i,j} = \frac{2}{(\Delta y)^2}\left[\Delta t\frac{E(1-\nu)}{(1+\nu)(1-2\nu)} - (\mu_1+\mu_2)\right] + \frac{2}{(\Delta x)^2}\left[\Delta t\frac{E}{2(1+\nu)} - \frac{\mu_1}{2}\right],$$
$$\beta^v_{i,j-1} = \beta^v_{i,j+1} = -\frac{1}{(\Delta y)^2}\left[\Delta t\frac{E(1-\nu)}{(1+\nu)(1-2\nu)} - (\mu_1+\mu_2)\right],$$
$$\beta^v_{i-1,j} = \beta^v_{i+1,j} = -\frac{1}{(\Delta x)^2}\left[\Delta t\frac{E}{2(1+\nu)} - \frac{\mu_1}{2}\right],$$
$$c^L = \frac{1}{4\Delta x\Delta y}\left(\frac{\mu_1}{2} + \mu_2 - \Delta t\frac{E}{2(1+\nu)(1-2\nu)}\right).$$

Finally,

(50)
$$f^k_{(j-1)M+i} = \frac{\Delta t}{2\Delta x}\left(\frac{\tau^k_{i-1,j}n^k_{i-1,j}\rho^k_{i-1,j}}{1+\lambda(n^k_{i-1,j})^2} - \frac{\tau^k_{i+1,j}n^k_{i+1,j}\rho^k_{i+1,j}}{1+\lambda(n^k_{i+1,j})^2}\right),$$
$$f^k_{MN+(j-1)M+i} = \frac{\Delta t}{2\Delta y}\left(\frac{\tau^k_{i,j-1}n^k_{i,j-1}\rho^k_{i,j-1}}{1+\lambda(n^k_{i,j-1})^2} - \frac{\tau^k_{i,j+1}n^k_{i,j+1}\rho^k_{i,j+1}}{1+\lambda(n^k_{i,j+1})^2}\right).$$

This leads to a $2MN \times 2MN$ linear system given by

$$\mathcal{A}U^{k+1} = \mathcal{B}U^k + f^k, \tag{51}$$

where U^k is a vector of length $2MN$ defined by

(52)
$$U^k = (u^k_{1,1}, \ldots, u^k_{M,1}, \ldots, u^k_{1,N}, \ldots, u^k_{M,N}, v^k_{1,1}, \ldots, v^k_{M,1}, \ldots, v^k_{1,N}, \ldots, v^k_{M,N}) :$$

f^k is a vector of length $2MN$ whose components are f^k_l, $1 \le l \le 2MN$. Finally, $\mathcal{A}$ and $\mathcal{B}$ are $2MN \times 2MN$ band matrices whose entries are given by $\alpha^u_{i,j}$, $\alpha^v_{i,j}$ and $\beta^u_{i,j}$, $\beta^v_{i,j}$, respectively, for $1 \le i \le M$ and $1 \le j \le N$.

In our simulation, we choose the numbers of meshlines $M = 81$ and $N = 71$ and a time step $\Delta t = 0.1$, unless stated otherwise. These parameter values are chosen to adequately resolve and simulate the sharp increase or decrease of n and ρ which occurs during their evolution as t increases.

The values of the parameters listed in (4) are taken from [7]: $n_0 = 5.2 \times 10^3$(cells/ml), $\rho_0 = 1$(mg/ml) and $\mathbf{u}(x, y, 0) = (0, 0)$, $\mu_1 = 3.187 \times 10^7$(P), $\mu_2 = 2.12 \times 10^7$(P), $E = 7.649 \times 10^7$(Pa), $\nu = 0.2$ Also, we have taken $\lambda = 1.2 \times 10^6$. With these, we can compute $\tau_{critical} = 9.14 \times 10^6$ by using the formula (25).

4.2. Numerical Results. The numerical scheme described in Section 4.1 is implemented by using Matlab.

The figures shown in Fig. 2 - 4 represent a typical numerical solution $(n(t), \mathbf{u}(t), \rho(t))$ of (2), equipped with the boundary conditions (9)-(10) and the initial conditions (8), computed at $t = 1.5$ and $t = 4.5$. Their intersections with the plane $y = 0.5$, that is, the graphs of $n(x, 0.5, t)$ for $x \in [0, 10]$, are presented in Fig. 5 in order to provide better visual aides for the time-evolution of the cell density n.

In Figures 2 - 4, the right half of the domain $[x^*, 10] \times [0, 1]$ corresponds to the somitic region where the traction function $\tau(x, y) > \tau_{critical}$ and the left half $[0, x^*] \times [0, 1]$ corresponds to the PSM where the traction function remains below $\tau_{critical}$-plane. As shown in Fig. 2a - Fig. 2b, our numerical simulations show the increase in the cell density n over the somitic region, accompanied by the simultaneous decrease in n over the region centered at x^*. The increase in n confirms the result obtained from performing the linear stability analysis in Sec 3.1 and corresponds to the formation of a somite. The decrease of n suggests the formation of the boundary of a somite.

Furthermore, it should be observed in Fig. 2a - Fig. 3b that the aggregation of cells and the variation of the ECM occur simultaneously, which agrees with the experimental data indicating the deformation of the ECM induced by the contractile force generated by the cells [17]. The vector fields of the displacement vector $\mathbf{u}$ shown in Fig. 4a - Fig. 4b show that the ECM is compressed and aligned due to the cell tractile forces and is drawn in the directions of the net contractile force vector, hence, toward the region where the values of n are greater.

Fig. 5 provides a better description of the time-evolution of our numerical solution n as t increases. The process of the cell aggregation starts off to the left of the boundary line $x = x^*$ which separates the somitic region from the PSM. The initial increase in n is observed near $x = 7.195$. Once n grows sufficiently large, the peak of n starts migrating toward the right boundary $x = 10$ of the domain Ω, as it increases in the height. This observation is explained by the motile activity of the cells in response to the variation of the concentration of the adhesive sites. According to our numerical data, the migration of the peak of n begins around $t = 4.6$.

Moreover, it should also be noted that in Fig. 5a, the separation of a somite from the PSM is observed in our numerical simulations, just before the migration of the cells starts; Over the region centered at $x = x^*$, n decreases and becomes approximately zero. This numerical observation can correspond to the physical separation of the tissue observed in vivo [9].

We have so far focused on the effect of the contractile forces generated by the cells, hence, on the traction function (3) and the parameters τ_{som} and τ_{psm} involved in its definition. However, there is another control parameter λ, whose effect is yet to be investigated. We hereby present here, as a remark, the two graphs below, hoping to shed some light on the role of λ in this problem. Fig. 6a and Fig. 6b are, respectively, the followings graphs:

$$\left\{ (\lambda,\, c) : c = \max_{x \in [0, L_1]} n(x, 0.5, 5.5 : \lambda) \right\} \tag{53}$$

and

$$\left\{ (\lambda,\, c) : c = \min_{x \in [0, L_1]} n(x, 0.5, 5.5 : \lambda) \right\} \tag{54}$$

where $n(x, 0.5, 5.5 : \lambda)$ denotes the first component of a solution of (2) for given λ. These graphs indicate that $\max\{\, n(x, 0.5, 5.5) : 0 \le x \le 10 \,\}$ increases and $\min\{\, n(x, 0.5, 5.5) : 0 \le x \le 10 \,\}$ decreases, exponentially as λ increases.

5. Conclusion

Our numerical results indicate that, in response to the traction forces exerted by the cells onto the ECM, the mechanochemical model can indeed give rise to the formation of a somite and its separation from the rest of the PSM. Moreover,

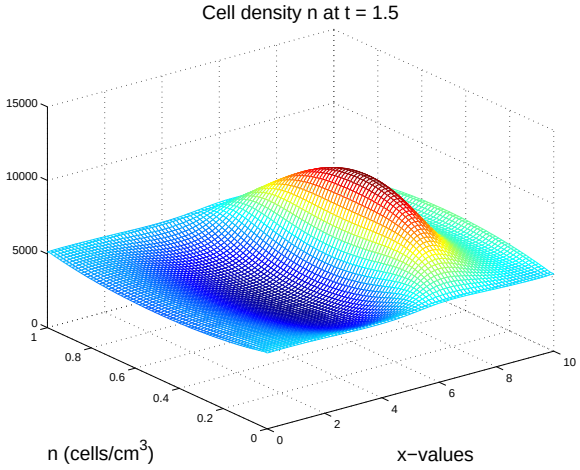

(A) n

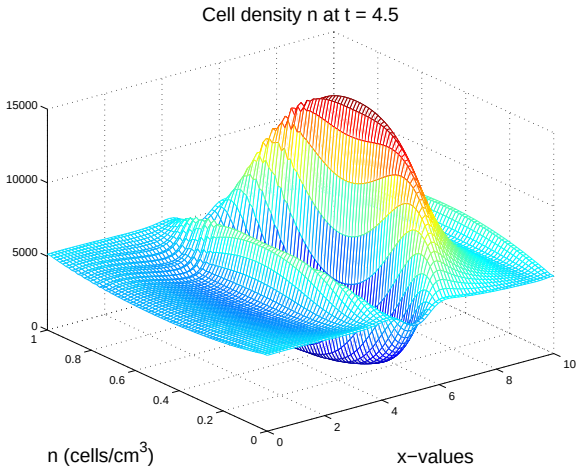

(B) n

FIGURE 2. $n_0 = 5.2 \times 10^3$(cells/ml), $\rho_0 = 1$(mg/ml) and $\mathbf{u}(\mathbf{x}, 0) = (0, 0)$, $\mu_1 = 3.187 \times 10^7$(P), $\mu_2 = 2.124 \times 10^7$(P), $E = 7.649 \times 10^7$(Pa), $\nu = 0.2$, $\lambda = 1.2 \times 10^{-6}$, $\tau_{som} = 1.27 \times 10^7$, and $\tau_{psm} = 2.74 \times 10^6$.

our numerical scheme with the particular parameter values can simulate some phenomena observed in vivo, such as the migration of the cells driven by their own contractile force and the interaction between the cells and the ECM. What it does not show is the roundness of a somite. It should also be noted that the value of λ can be adjusted to manipulate the amplitude of the cell density, although its physical significance in the formation of a somite is not clear.

In summary, as our numerical results suggest, the mechanochemical model well captures the key mechanical properties of the cells and the ECM, involved in forming a somite. This suggests the validity of deploying the mechanochemical model to simulate the formation of a somite and/or somitogenesis.

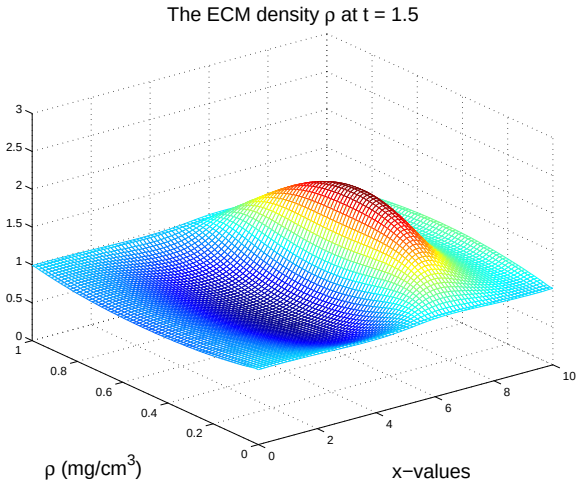

(A) ρ

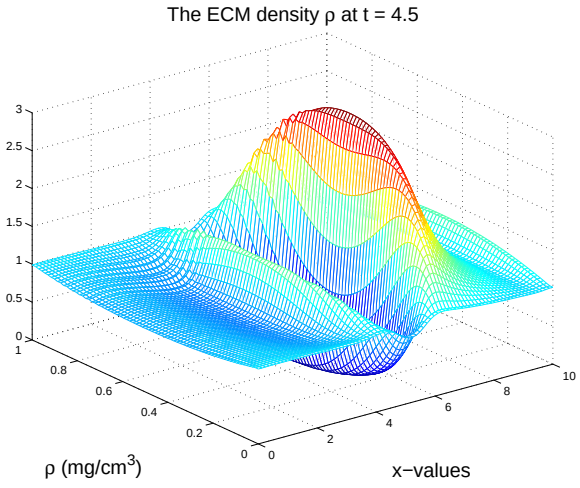

(B) ρ

FIGURE 3. $n_0 = 5.2 \times 10^3$(cells/ml), $\rho_0 = 1$(mg/ml) and $\mathbf{u}(\mathbf{x}, 0) = (0, 0)$, $\mu_1 = 3.187 \times 10^7$(P), $\mu_2 = 2.124 \times 10^7$(P), $E = 7.649 \times 10^7$(Pa), $\nu = 0.2$, $\lambda = 1.2 \times 10^{-6}$, $\tau_{som} = 1.27 \times 10^7$, and $\tau_{psm} = 2.74 \times 10^6$.

Acknowledgments

This work was partially supported by the National Science Foundation under the grant NSF-DMS-0906440, and by the Research Fund of Indiana University. The author thanks S. Schnell for suggesting this study and R. Grima for useful and interesting discussions.

References

[1] R.E. Baker, S. Schnell, P.K. Maini, Mathematical models for somite formation, Current topics in developmental biology, 81:183-203, 2008.

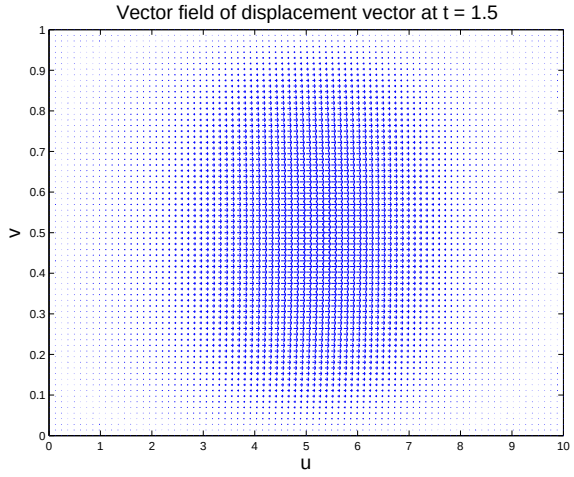

(A) **u**

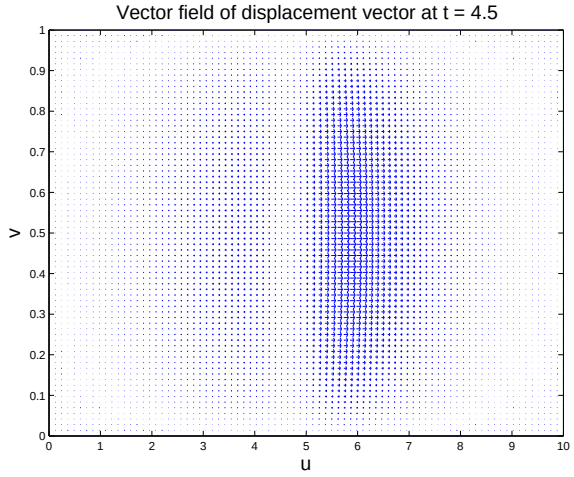

(B) **u**

FIGURE 4. $n_0 = 5.2 \times 10^3$(cells/ml), $\rho_0 = 1$(mg/ml) and $\mathbf{u}(\mathbf{x}, 0) = (0, 0)$, $\mu_1 = 3.187 \times 10^7$(P), $\mu_2 = 2.124 \times 10^7$(P), $E = 7.649 \times 10^7$(Pa), $\nu = 0.2$, $\lambda = 1.2 \times 10^{-6}$, $\tau_{som} = 1.27 \times 10^7$, and $\tau_{psm} = 2.74 \times 10^6$.

[2] J.R. Collier, D. McInerney, S. Schnell, P.K. Maini, D.J. Gavaghan, P. Houston, C.D. Stern, A cell cycle model for somitogenesis mathematical formulation and numerical solutions, J. Theor. Biol., 207:305-316, 2000.

[3] J. Cookee, E.C. Zeeman, Aclock and wavefront model for control of the number of repeated structures during animal morphogenesis, J. Theor. Biol., 58:455-476, 1976

[4] G.C. Cruywagen, J.D. Murray, On a tissue interaction model for skin pattern formation, J. Nonlinear Sci., 2:217-240, 1992.

[5] ,J. Dubrulle, M.J. McGrew, O. Pourquié, FGG signaling controls somite boundary position and regulates segmentation clock control of spatiotemporal Hox gene activation, Cell, 106:219-232, 2001.

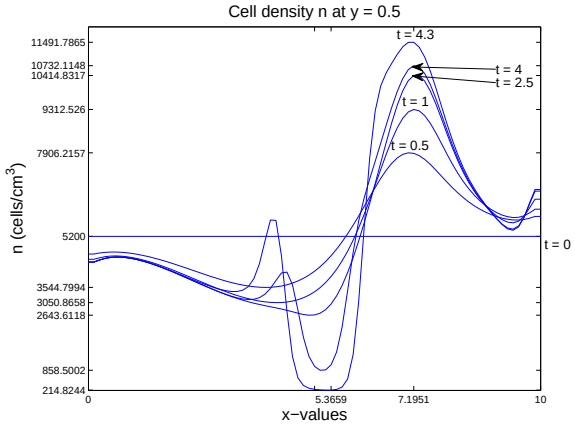

(A) $n(x, 0.5, t)$ for $t = 0$, 0.5, 1, 2.5, 4, 4.3

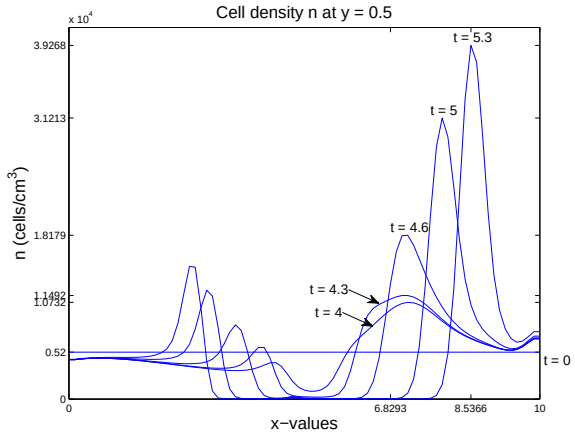

(B) $n(x, 0.5, t)$ for $t = 4.0$, 4.3, 4.6, 5, 5.3

FIGURE 5. $n_0 = 5.2 \times 10^3$(cells/ml), $\rho_0 = 1$(mg/ml) and $\mathbf{u}(x, y, 0) = (0, 0)$, $\mu_1 = 3.187 \times 10^7$(P), $\mu_2 = 2.124 \times 10^7$(P), $E = 7.649 \times 10^7$(Pa), $\nu = 0.2$, $\lambda = 1.2 \times 10^{-6}$, $\tau_{som} = 1.27^7$, and $\tau_{psm} = 2.74 \times 10^6$.

[6] J. Dubrulle, M.J. McGrew, O. Pourquié, From head to tail: links between the segmentation clock and antero-posterior patterning of the embryo. Curr. Opin. Genet. Dev., 12:519-523, 2002.

[7] I. Ferrenq, L. Tranqui, B. Vailhé, P.Y. Gumery, P. Tracqui, Modelling biological gel contraction by cells: mechanocellular formation and cell traction force quantification. Acta Biotheor., 45:267-293, 1997.

[8] S.F. Gilbert, Developmental biology, Sinauer associates, Inc., Sunderland, Massachusetts, Sixth edition, 2000.

[9] P.M. Kulesea, S. Schnell, S. Rudloff, R.E. Baker, P.K. Maini, From segment to somite: segmentation to epithelialization analyzed within quantitative frameworks, Dev. Dynam., 236(6):1392-1402, 2007.

[10] A mechanical model of angiogenesis and vasculogenesis, Mathematical modeling and numerical analysis, 37(4):581-599, 2003.

[11] D. McInerney, S. Schnell, R.E. Baker, P.K. Maini, Mathematical formulation for the cell cycle model in somitogenesis: parameter constraints and numerical solutions, IMA, Math. Med. Biol., 21:85-113, 2004.

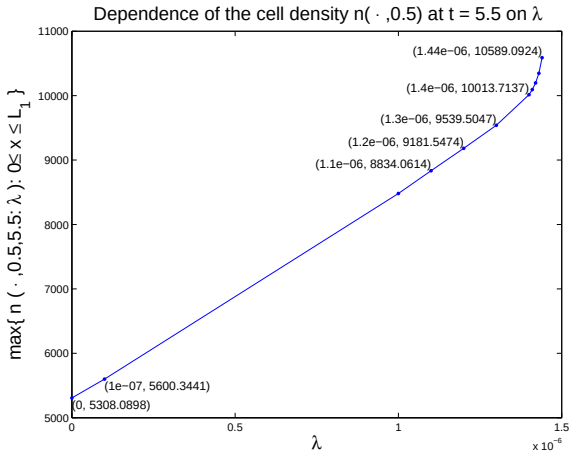

(A) $\{(\lambda,\, c) : c = \max_{x\in[0,L_1]}\, n(x, 0.5, 5.5 : \lambda)\}$

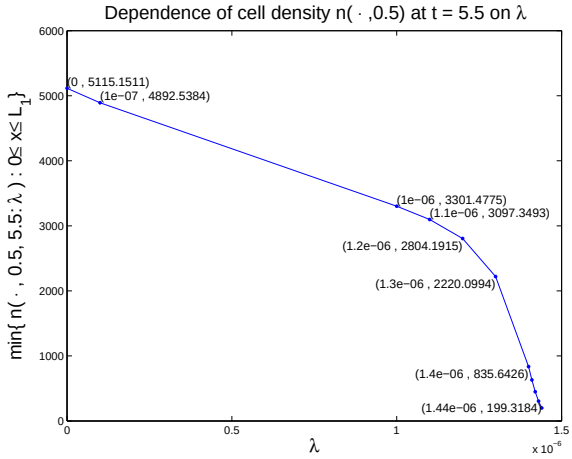

(B) $\{(\lambda,\, c) : c = \min_{x\in[0,L_1]}\, n(x, 0.5, 5.5 : \lambda)\}$

FIGURE 6. $n_0 = 5.2 \times 10^3$(cells/ml), $\rho_0 = 1$(mg/ml) and $\mathbf{u}(x, y, 0) = (0, 0)$, $\mu_1 = 3.187 \times 10^7$(P), $\mu_2 = 2.124 \times 10^7$(P), $E = 7.649 \times 10^7$(Pa), $\lambda = 1.0 \times 10^6$ $\nu = 0.2$, $\tau_{som} = 6.42 \times 10^6$ and $\tau_{psm} = 3.21 \times 10^6$.

[12] H. Meinhardt, Models of segmentation, Plenum press, New York, 179-189, 1986.
[13] J.D. Murray, On the mechanochemical theory of biological pattern formation with application to vasculogenesis, C.R. Biologies, 326:239-252, 2003.
[14] J.D. Murray, P.K. Maini, A new approach to the generation of pattern and form in embrylogy, Sci. Prog., 70:539-553, 1986.
[15] J.D. Murray, P.K Maini, R.T. Tranquillo, Mechanochemical models for generating biological pattern and form in development, Phys. Rep., 171(2):59-84, 1988.
[16] G. Oster, J.D. Murray, Pattern formation and developmental constraints, J. Exp. Zool., 251:186-202, 1989.
[17] G. Oster, J.D. Murray, A.K. Harris, Mechanical aspects of mesenchymal morphogenesis, J. Embryol. Exp. Morph., 78:83-125, 1983.

[18] G. Oster, J.D. Murray, P.K. Maini, A model for chondrogenic condensations in the developing limb - the role of extracellular matrix and cell tractions, J. Embryol. Exp. Morph., 89:93-112, 1983.
[19] A.A. Polezhaev, A mathematical model fo the mechanism of vertebrate somitic segmentation, J. Theor. Biol., 156:169-181, 1992.
[20] Polezhaev, A. A., Mathematical model of segmentation in somitogenesis in vertebrates, Biophysics, 40:583-589, 1995.
[21] D.R.N. Primmentt, W.E. Norris, G.J. Carlson, R.J. Keynes, C.D. Stern, Periodic anomalies induced by heat shock in the chick embryo are associated with the cell cycle, Development, 105:119-130, 1989.
[22] D.R.N. Primmentt, C.D. Stern, R.J. Keynes, Heat Schock repeated segmental anomalises in the chick embryo, Development, 104:331-339, 1988.
[23] S. Schnell, P.K. Maini, D. McInterney, D.J. Gavaghan, P. Houston, Models for pattern formation in somitogenesis: a marriage of cellular and molecular biology, C.R. Biologies, 325:179-189, 2002.
[24] M.S.J. Stickney, H.L. Barresi, S.H. Devoto, Somite development in zebrafish, Dev. Dynam., 219(2):287-303, 2000.
[25] F.E. Stockdale, W. Nikovits, B. Christ, Molecular and cellular biology of avian somite development, Dev. Dynam., 219(3):304321, 2000.

18-20 Avenue De La République 92400 Courbevoie, France
E-mail: ygcaillieret@gmail.com